

# Valence and Core–Valence Effects in $N$ -Like Kr, Rb and Sr Ions

L.H. HAO, H. FENG\* AND X.P. KANG

School of Science and Technology, Qiongzhou University, Hainan 572022, China

(Received December 17, 2013)

Energy levels, wavelengths, transition rates and line strengths are reported for the  $2s^22p^3$ – $2s2p^4$  transition array in Kr(XXX), Rb(XXXI) and Sr(XXXII). Wave functions were determined using the multiconfiguration Dirac–Fock method with account for valence and core–valence correlation effects. The present results are presented and compared with experimental data and with values from other calculations. The calculated values including core–valence correlation are in good agreement with other available theoretical and experimental values, and therefore can be used for the further astrophysical investigations.

DOI: [10.12693/APhysPolA.127.693](https://doi.org/10.12693/APhysPolA.127.693)

PACS: 31.30.Gs, 32.30.–r

## 1. Introduction

Intercombination lines are being increasingly used as an injected impurity for diagnosing tokamak fusion plasmas. Due to the high temperatures of such plasmas ( $>10^6$  K), many of its ionization stages are accessible. Therefore, in view of the forthcoming ITER project, atomic data (namely energy levels, line strengths or radiative decay rates, collision strengths, etc.) are required for many ions in order to estimate the power loss from the impurities. Additionally, these lines are especially important since spectral line intensity ratios, particularly in the XUV region, may be useful in determining the production rate and concentration of the alpha particles produced in a burning DT plasma. However, to model these experiments, accurate atomic data are required, and one must depend on theoretical results since measured values are generally not available.

Atomic data available in the literature are either confined to a few levels/transitions, or are of limited accuracy. Many theoretical studies of transitions in  $N$ -like ions have been made during the past 20–30 years, especially for electric-dipole ( $E1$ ) transitions within the  $n = 2$  complex of states. Energy levels, transition rates and oscillator strengths for  $N$ -like ions have been calculated using multi-configuration Dirac–Fock (MCDF) [1–3], relativistic distorted-wave [4], the Dirac–Fock (DF) approximation [5], and relativistic many-body perturbation theory (MBPT) combined with configuration interactions (CI) [6] methods. A correspondingly few of experimental studies of wavelengths of  $n = 2$  states has been made using beam foil techniques [7, 8]. Critical data compilations based on available theoretical sources are given in [9–11]. We refer to these compilations as recommended National Institute of Standards and Technology (NIST) data later in the following sections.

In this paper, we describe the computational procedures used for the different isoelectronic sequences and discuss the accuracy of the results for selected cases. All calculations convergence can be monitored. Each calculation is characterized by parameters  $n$  and  $l$  that refer to the maximum principal and orbital quantum numbers of the orbital set used to determine the expansion. Typically, the same expansions are used for all members of a sequence. In spectrum calculations for sequences where several hundred levels may be computed, the labels of levels are computer generated from the intermediate coupling wave-function expansion. As a first approximation, the label is the configuration state function (CSF) with the largest expansion coefficient. When this scheme assigns the same label to two different eigenstates, a detailed analysis is performed. The  $LS$  value is that of the largest term composition and then, within the expansion for this term, the configuration states are determined as described earlier [12].

Not only are the  $N$ -like  $2s2p^4$   $^2S_{1/2}$  –  $2s^22p^2$   $^2P_{1/2,3/2}$   $E1$  lines, in combination with other transitions, important in electron temperature and density diagnostics but the relative intensity of these two transitions provides a good indication of the optical depth of the source, since they originate from the same upper level. Since both the lifetime and the branching ratio are directly measurable, with very few assumptions for the observed plasma, they are also excellent test cases for atomic theoretical models and experimental methods.

The theory provides us with computed transition rates

$$A_1 = A(2s2p^4 \ ^2S_{1/2} - 2s^22p^3 \ ^2P_{1/2})$$

$$\text{and } A_2 = A(2s2p^4 \ ^2S_{1/2} - 2s^22p^3 \ ^2P_{3/2}), \quad (1)$$

while the measurable and, for diagnostics, interesting properties are the branching ratio

$$Q = \frac{A_2}{A_1} \quad (2)$$

and the lifetime

\*corresponding author; e-mail: [feng\\_h007@126.com](mailto:feng_h007@126.com)

$$\tau = \frac{1}{A_1 + A_2}. \quad (3)$$

The aim of the present paper is to extend our systematic approach to include new effects and to mainly concentrate on the medium end of the sequence, where correlation effects are most important. We will investigate the importance of valence–valence correlation, which so far has not been included explicitly in any of the calculations for medium- $Z$  ions. We will also focus on the branching ratio of the two lines, which serves as a complimentary test of our calculations. An important part of our approach is an attempt to define a method to estimate uncertainties in *ab initio* calculations and apply them to our and, when possible, others calculations. Our method of choice is the *ab initio* MCDF active set approach [13]. Different types of MCDF approaches are classified according to the functional used in the optimization stage. In this work we exclusively use the extended optimal level (EOL) approach, where the functional is defined as a linear combination of a few important eigenvalues to the energy matrix. As represented by the GRASP2K codes originating in Oxford [14] and further developed by Jönsson et al. [15]. It is a modification and extension of the GRASP92 codes by Parpia et al. [16].

In summary, this work presents both a systematic calculation of the fine structure, transition rates, wavelengths, and line strengths between excited states in  $N$ -like ions and a study of the importance of the correlation corrections to those properties. Our data are compared with the existing measurements.

## 2. Theoretical atomic structure methods

The basic ideas for this approach have been described elsewhere [15–17], so let us here only summarize some important concepts for the present case. In an MCDF calculation, the atomic state function is represented by a linear combination of configuration state functions (CSF's),

$$\psi(\gamma J) = \sum_i c_i \Phi_i(\alpha, J). \quad (4)$$

The CSF's are generated by excitations from the reference configuration to the active set of orbitals. We divided up the calculations into two parts, one where we optimized a set of orbitals for the even states and one for the odd states, i.e. the upper and lower states were described by two independently optimized sets of orbitals. Because of this we had to use biorthogonal transformation [17] of the atomic state functions to calculate the transition parameters. By restricting the way excitations can be done, different correlation effects can be studied. The size of the active set determines to what accuracy these correlation effects are represented in the wave function.

In the present work, valence–valence (VV) and core–valence (CV) electron correlation effects were included to describe inner properties, like fine structure. The theoretical basis of our present computational approach has been discussed in our previous work [12]. In this paper, the correlation is represented by different constraints on

the generation of the CSFs included in Eq. (1). If we only include the VV correlation, the core electrons are kept fixed in all the CSFs generated. To include the CV correlation, we allow one of the core electrons to be excited to generate the CSFs. In an early work on silicon-like ions [18] they treated valence correlation in these systems, using the MCDHF method. Let us briefly outline the main steps in these calculations.

We performed a series of calculations which increased in complexity as more orbitals and, consequently, more CSFs were added. All valence correlation calculations involve a set of CSFs generated by allowing single- and double-electron replacements from the multireference set:

$$\text{even parity : } 1s^2 2s 2p^4$$

$$\text{odd parity : } 1s^2 2s^2 2p^3$$

with the  $1s^2$  core remaining closed. The final symmetries included were  ${}^2P$ ,  ${}^4S^o$ ,  ${}^2D^o$  and  ${}^2P^o$ .

The stepwise procedure, based on the active set of orbitals, can be described as

$n = 3$ . The core orbitals  $1s$ , together with the active set  $2s$ ,  $2p$ ,  $3s$ ,  $3p$ , and  $3d$  orbitals, were included to generate the lowest complexes of configurations.

$n = 4$ . The  $4s, 4p, 4d$  and  $4f$  were added to the active set, and only these new orbitals were optimized. The generation of CSF followed the distribution  $\{2\}^2\{2, 3, 4\}^3$ , which implies that two of the orbitals always belonged to the  $n = 2$  set, while three had  $n = 2, 3$  or  $4$ .

$n = 5$ . The active set was augmented by the  $5s$ ,  $5p$ ,  $5d$ , and  $5f$ , which were optimized, and the CSF were generated according to the distribution  $\{2\}^2\{2, 3, 4, 5\}^3$ .

$n = 6$ . Finally the  $6s$ ,  $6p$ ,  $6d$ , and  $6f$  were added and the CSF followed the distribution  $\{2\}^2\{2, 3, 4, 5, 6\}^3$  giving a total number of 43308CSF.

The opening of the  $1s$  shell in the core–valence correlation (core polarization) calculations leads to a considerable increase in the number of CSFs, by including CSFs which only had one electron in the  $1s$  shell. We also increased the number of calculations by allowing more than two electrons in orbitals with  $n = 2$  or higher.

$n = 3$ . The core orbitals  $1s$ , together with  $2s$ ,  $2p$ ,  $3s$ ,  $3p$ , and  $3d$  orbitals were included in the active set, produced CSF generated according to  $\{2, 3\}^5$ .

$n = 4$ . The  $4s$ ,  $4p$ ,  $4d$ , and  $4f$  were added to the active set, and only the new orbitals were optimized. The generation of CSF followed the distribution  $\{2, 3, 4\}^5$ , with the limitation that we only allowed two electrons in the  $4f$  orbital.

$n = 5$ . In this step we added core–valence correlations from the  $1s$  orbital. The active set was augmented by  $5s$ ,  $5p$ , and  $5d$ , which were optimized. The CSF included were those from the last step plus those generation according to  $\{1s\}^1\{2s, 2p\}^1\{2, 3, 4, 5\}^5$  with the limitation that  $4f$  was not included.

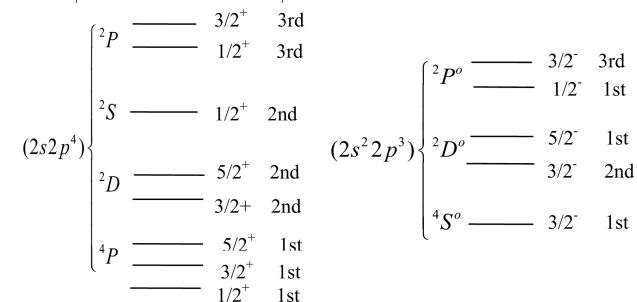
$n = 6$ . Finally the  $6s$ ,  $6p$ ,  $6d$ , and  $6f$  were added and the CSF followed the distribution  $\{2, 3, 4, 5, 6\}^5$  with the limitation that we only allowed two electrons in  $4f$  and  $5f$ , plus  $\{1s\}^1\{2s, 2p\}^1\{2, 3, 4, 5\}^5$  with the limitation that  $4f$  and  $5f$  were not included.

At this point, the number of configurations was more than 120,000, and adding another layer of orbitals increased the number to more than 150,000 and the calculation became too big to be dealt with in the normal way.

### 3. Results and discussion

In this section we show some values for theoretical energy levels, transition rates and line strengths, while considering the convergence and accuracy of our calculation and comparing the three results (i.e. VV and CV). We will discuss errors or uncertainties in these calculated values and calculations of the *A* values for the  $2s2p^4\ ^2S_{1/2} - 2s^22p^2\ ^2P_{1/2,3/2}$  *E1* lines.

To assist readers in identifying energy levels and locating transitions, we present schematic diagrams of energy levels, with their labels, for *N*-like ions in



The relative positions of energy levels in these figures resemble those in actual spectra of light ions, although some of these levels are rearranged as *Z* increases along isoelectronic sequences.

In Table I we give the relativistic (*LSJ*) excitation energies for the largest of the core-valence correlation calculations ( $n \leq 6$ ) together with other calculations [1, 3, 19, 20]. Many of the calculated levels in the core-valence correlation  $n \leq 5$  calculation look in reasonable agreement with other calculations, however, it is necessary to increase the orbital set further to represent the states to a similar extent and to induce stability in the ground state. These results obtained by looking for a smooth difference between all presented transition energies and the corresponding energies from a simple single configuration calculation. In spite of the fact that the core-valence correlation approach seemed to converge, there were signs of significant uncertainties. For Kr(XXX), the computed ( $487679\text{ cm}^{-1}$ ) fine structure of the ground term deviated clearly from the NIST [20] ( $487220\text{ cm}^{-1}$ ) (see Table I). The same was true for the term splitting between  $^4P^e$  and  $^2D^e$  which was off by about 0.05–0.1%. Comparison with known energy differences is one of our most important tools to determine uncertainties in the calculations, so we concluded that our CV calculations were associated with large uncertainties with other results (up to 2%, as we will see below). The reason was interpreted as a systematic error-left-out correlation.

TABLE I

*LS ab initio* excitation energies [*E* in  $\text{cm}^{-1}$ ] in Kr(XXX) for CV calculations.

Level	<i>n</i> = 5	<i>n</i> = 6	NIST <sup>b</sup>	GRASP <sup>c</sup>	GRASP <sup>d</sup>	FAC <sup>e</sup>	FAC <sup>f</sup>	MCDF <sup>g</sup>
	CV <sup>a</sup>							
$2s^22p^3\ ^4S_{3/2}$	0	0	0	0	0	0	0	0
$^2D_{3/2}$	385096	385044	384900	390932	384692	384856	385606	380578
$^2D_{5/2}$	488440	487673	487220	504203	488962	488870	488567	484773
$^2P_{1/2}$	622489	622203	621500	628154	622679	622068	622642	619605
$^2P_{3/2}$	996272	996384		1012305	995486	995382	995557	992888
$2s2p^4\ ^4P_{5/2}$	1391306	1390905	1391300	1407711	1395305	1395544	1395965	1385723
$^4P_{3/2}$	1648219	1647393	1646580	1665438	1653365	1653478	1653680	1644638
$^4P_{1/2}$	1659238	1658747	1657500	1672859	1665060	1664878	1665359	1655030
$^2D_{3/2}$	1959015	1957306	1955480	1980460	1966913	1966563	1966335	1959228
$^2D_{5/2}$	2076163	2074460		2106469	2084094	2083650	2083408	2076507
$^2P_{3/2}$	2321736	2318497	2318860	2352214	2332797	2332041	2331212	2326101
$^2P_{1/2}$	2234462	2232436		2256955	2243953	2243173	2243013	2235491
$^2S_{1/2}$	2744519	2742366		2776665	2754200	2753313	2753003	2746345

<sup>a</sup>Core-valence correlation included.

<sup>b</sup>Taken from [20].

<sup>c</sup>Coulomb energies, Aggarwal et al. [1].

<sup>d</sup>QED-corrected energies, Aggarwal et al. [1].

<sup>e</sup>Energies from the flexible atomic code (FAC) of Gu [19] for 272 level calculations.

<sup>f</sup>Energies from FAC for 668 level calculations, Gu [19].

<sup>g</sup>Cheng et al. [3]

TABLE II

MCDF excitation energies [ $\text{cm}^{-1}$ ] in Rb(XXXI). Results of considering VV and CV correlations include Breit interaction and quantum electrodynamical (QED) effects.

Level	VV <sup>a</sup>	CV <sup>b</sup>	MCDF <sup>c</sup>	CI+MBPT <sup>d</sup>
$2s^2 2p^3 \ ^4S_{3/2}^o$	0	0	0	0
$\ ^2D_{3/2}^o$	436951	437079	437900	437090
$\ ^2D_{5/2}^o$	544379	544313	546800	544213
$\ ^2P_{1/2}^o$	684065	684046	682300	684171
$\ ^2P_{3/2}^o$	1113349	1114048	1112600	1113739
$2s2p^4 \ ^4P_{5/2}$	1483743	1483720	1483200	1483697
$\ ^4P_{3/2}$	1762616	1762512	1765200	1762176
$\ ^4P_{1/2}$	1769743	1769094	1771400	1769354
$\ ^2D_{3/2}$	2097793	2096761	2104000	2096606
$\ ^2D_{5/2}$	2227967	2227131	2234900	2226880
$\ ^2P_{3/2}$	2479319	2477582	2492700	2476654
$\ ^2P_{1/2}$	2389915	2388778	2398500	2388215
$\ ^2S_{1/2}$	2957445	2956573	2967400	2955626

<sup>a</sup>Valence correlation calculation.

<sup>b</sup>Core-valence correlation included.

<sup>c</sup>Zhang et al. [4]

<sup>d</sup>Gu [6].

TABLE III

MCDF excitation energies [ $\text{cm}^{-1}$ ] in Sr(XXXII). VV and CV correlations include Breit interaction and quantum electrodynamical (QED) effects.

Level	VV <sup>a</sup>	CV <sup>b</sup>	MCDF <sup>c</sup>	CI+MBPT <sup>d</sup>
$2s^2 2p^3 \ ^4S_{3/2}^o$	0	0	0	0
$\ ^2D_{3/2}^o$	494980	495116	496000	495259
$\ ^2D_{5/2}^o$	607061	607176	609300	606881
$\ ^2P_{1/2}^o$	752585	753025	750600	752555
$\ ^2P_{3/2}^o$	1242776	1243445	1241900	1243118
$2s2p^4 \ ^4P_{5/2}$	1581605	1580698	1581300	1581814
$\ ^4P_{3/2}$	1882386	1881259	1885800	1881974
$\ ^4P_{1/2}$	1886037	1885355	1888000	1885692
$\ ^2D_{3/2}$	2249824	2248796	2255200	2248907
$\ ^2D_{5/2}$	2392677	2391779	2399400	2391700
$\ ^2P_{3/2}$	2650956	2649059	2663900	2648329
$\ ^2P_{1/2}$	2559261	2557925	2967400	2557892
$\ ^2S_{1/2}$	3189696	3188668	3199000	3187096

<sup>a</sup>Valence correlation calculation.

<sup>b</sup>Core-valence correlation included.

<sup>c</sup>Zhang et al. [4].

<sup>d</sup>Gu [6].

In Tables II and III computed energies for Rb(XXXI) and Sr(XXXII) are compared with the multiconfiguration Dirac-Fock (MCDF) given by Zhang et al. [4] and a combination of configuration interaction method (CI) with many-body perturbation theory (MBPT) given by Gu [6]. From Tables II and III, it is clear that including the CV correlation results show excellent agreement with the theoretical values of Gu [6] to within a few percentage points (0.0624% and 0.0025%). Also, our calculations are also generally in good agreement with the MCDF results

of Zhang et al. [4]. However, a more detailed comparison of the calculated and the CI+MBPT energies [6] for these transitions (Tables II and III) indicates that some splitting energies given by our GRASP2 K calculations are in better agreement with the CI+MBPT energies [6] than the MCDF results of Zhang et al. [4]. Specifically, the maximum difference between the results of CI+MBPT [6] and our GRASP2 K splitting energies is 0.062%, but the maximum difference for the MCDF results of Zhang et al. [4] and the CI+MBPT results [6] is 0.473%. In the work presented here we have increased the number of configurations included or the size of the orbital set in a systematic manner until good convergence was obtained. This difference in the two methods should account for a large fraction of the disagreement in the results.

TABLE IV

$LS$  convergence trends for the  $2s^2 2p^3 \ ^2P_{1/2}^o - 2s2p^4 \ ^2P_{1/2}$  transition for  $Z = 36-38$  as a function of the maximum  $n$  in the orbital set used in determining the CSF expansion. The number in brackets represents the power of 10.

$n$	Kr(XXX)		Rb(XXXI)		Sr(XXXII)	
	$S_L$	$S_V$	$S_L$	$S_V$	$S_L$	$S_V$
3	1.85(-2)	1.89(-2)	1.79(-2)	1.85(-2)	1.35(-2)	1.46(-2)
4	1.83(-2)	1.86(-2)	1.76(-2)	1.82(-2)	1.32(-2)	1.41(-2)
5	1.82(-2)	1.84(-2)	1.74(-2)	1.79(-2)	1.30(-2)	1.38(-2)
6	1.82(-2)	1.83(-2)	1.72(-2)	1.76(-2)	1.29(-2)	1.36(-2)
Ref.	1.81(-2) <sup>a</sup>		1.71(-2) <sup>b</sup>		1.28(-2) <sup>b</sup>	

<sup>a</sup>Aggarwal et al. [1].

<sup>b</sup>Taken from [20].

In Table IV the line strengths ( $S$ ) for  $2s^2 2p^3 \ ^2P_{1/2}^o - 2s2p^4 \ ^2P_{1/2}$  transition for  $Z = 36-38$  are shown as functions of increasing active sets and multireference sets. The results are from the various CV correlation calculations. The convergence of the results is clearly seen as  $n$  increases in the core-valence correlation calculations. The length and velocity forms agree well which is encouraging as these transitions were not the primary concern of this work. It is also encouraging to see that the agreement of the two gauges is very good and the near-equal values of the length and velocity of the transitions give an additional check on the accuracy of our results. At the same time, we can find that the length value is more stable in that it changes less as the active space extends. Strengths for all  $E1$  transitions in the  $2s^2 2p^3 - 2s2p^4$  transition array are given in Fig. 1.

In Fig. 1, we illustrate the  $Z$ -dependence of the differences between line strengths calculated in length  $S_L$  and velocity  $S_V$  forms for  $2s^2 2p^3 \ ^2P_{1/2}^o - 2s2p^4 \ ^2S_{1/2}$ ,  $2s^2 2p^3 \ ^2P_{1/2}^o - 2s2p^4 \ ^2P_{3/2}$  and  $2s^2 2p^3 \ ^2P_{3/2}^o - 2s2p^4 \ ^2S_{1/2}$  transitions. The ratio  $(S_L - S_V)/S_L$  for the  $2s^2 2p^3 \ ^2P_{1/2}^o - 2s2p^4 \ ^2S_{1/2}$  transition is about 3% for entire interval of  $Z$  with exception of  $Z = 37-39$  in both cases. The ratio  $(S_L - S_V)/S_L$  for the  $2s^2 2p^3 \ ^2P_{1/2}^o - 2s2p^4 \ ^2P_{3/2}$  transition is about 4.5% for all  $Z$ . The ratio  $(S_L - S_V)/S_L$  increases substantially (from 4.5%

to 5.5% for  $Z = 36-42$ ) for the  $2s^2 2p^3 2P_{3/2}^o - 2s 2p^4 2S_{1/2}$  transition. In view of the gauge dependence issue discussed above, our results below are presented in length form only to decrease the volume of tabulate material.

In Table V, we compare our results for wavelengths  $\lambda$ , transition probabilities  $A$  for selected transitions for Kr(XXX) with experimental data presented in [8]. We also compare our results with theoretical results obtained by Zhang et al. [4] who used the MCDF method

TABLE V

Wavelengths  $\lambda$  [Å], transition probabilities  $A$  [ $s^{-1}$ ] for  $LS$ -allowed transitions in Kr(XXX): (a) present, (b) GRASP data [1], (c) experimental data [8].

Lower level	Upper level	Kr(XXX)					
		$\lambda^a$ (VV)	$\lambda^a$ (CV)	$\lambda^b$	$\lambda^c$	$A^a$ (CV)	$A^b$
$2s^2 2p^3 4S_{3/2}$	$2s 2p^4 2S_{1/2}$	36.45	36.47	36.31		2.62(7)	2.51(7)
$2s^2 2p^3 2D_{3/2}$	$2s 2p^4 2S_{1/2}$	42.40	42.42	42.20		2.85(10)	3.04(10)
$2s^2 2p^3 4S_{3/2}$	$2s 2p^4 2P_{3/2}$	43.09	43.13	42.87		1.62(10)	1.71(10)
$2s^2 2p^3 2P_{1/2}$	$2s 2p^4 2S_{1/2}$	47.13	47.17	46.92		2.32(9)	2.51(9)
$2s^2 2p^3 4S_{3/2}$	$2s 2p^4 2D_{5/2}$	48.18	48.20	47.98		4.08(7)	3.98(7)
$2s^2 2p^3 4S_{3/2}$	$2s 2p^4 2D_{3/2}$	51.06	51.09	50.84		2.15(10)	2.32(10)
$2s^2 2p^3 2D_{3/2}$	$2s 2p^4 2P_{3/2}$	51.67	51.72	51.33		1.15(9)	1.38(9)
$2s^2 2p^3 2D_{5/2}$	$2s 2p^4 2P_{3/2}$	54.56	54.63	54.24	54.60	2.10(11)	2.19(11)
$2s^2 2p^3 2P_{3/2}$	$2s 2p^4 2S_{1/2}$	57.22	57.28	56.86		2.22(11)	2.32(11)
$2s^2 2p^3 2P_{1/2}$	$2s 2p^4 2P_{3/2}$	58.87	58.96	58.47		3.26(10)	3.36(10)
$2s^2 2p^3 2D_{3/2}$	$2s 2p^4 2D_{5/2}$	59.15	59.19	58.84		1.40(9)	1.42(9)
$2s^2 2p^3 4S_{3/2}$	$2s 2p^4 4P_{1/2}$	60.26	60.28	60.06	60.33	7.12(10)	7.33(10)
$2s^2 2p^3 4S_{3/2}$	$2s 2p^4 4P_{3/2}$	60.66	60.70	60.48	60.73	8.60(10)	8.71(10)
$2s^2 2p^3 2D_{5/2}$	$2s 2p^4 2D_{5/2}$	62.98	63.02	62.69		7.62(10)	7.94(10)
$2s^2 2p^3 2D_{3/2}$	$2s 2p^4 2D_{3/2}$	63.55	63.60	63.20	63.67	9.44(10)	9.81(10)
$2s^2 2p^3 2D_{5/2}$	$2s 2p^4 2D_{3/2}$	67.99	68.05	67.66		4.27(9)	4.35(9)
$2s^2 2p^3 4S_{3/2}$	$2s 2p^4 4P_{5/2}$	71.84	71.89	71.67	71.88	2.18(10)	2.27(10)
$2s^2 2p^3 2P_{1/2}$	$2s 2p^4 2D_{3/2}$	74.82	74.91	74.39		2.29(9)	2.47(9)
$2s^2 2p^3 2P_{3/2}$	$2s 2p^4 2P_{3/2}$	75.50	75.65	74.78		1.39(10)	1.45(10)
$2s^2 2p^3 2D_{3/2}$	$2s 2p^4 4P_{1/2}$	78.46	78.51	78.10		2.28(9)	2.43(9)
$2s^2 2p^3 2D_{3/2}$	$2s 2p^4 4P_{3/2}$	79.14	79.21	78.82		3.13(6)	3.28(6)
$2s^2 2p^3 2D_{5/2}$	$2s 2p^4 4P_{3/2}$	86.15	86.23	85.88	86.26	2.81(9)	2.72(9)
$2s^2 2p^3 2P_{3/2}$	$2s 2p^4 2D_{5/2}$	92.62	92.76	91.86		9.00(9)	9.43(9)
$2s^2 2p^3 2P_{1/2}$	$2s 2p^4 4P_{3/2}$	97.41	97.55	97.02		1.13(8)	1.34(8)
$2s^2 2p^3 2D_{3/2}$	$2s 2p^4 4P_{5/2}$	99.30	99.40	98.95		6.12(9)	6.29(9)
$2s^2 2p^3 2P_{3/2}$	$2s 2p^4 2D_{3/2}$	103.88	104.07	102.9		2.91(5)	2.09(5)
$2s^2 2p^3 2D_{5/2}$	$2s 2p^4 4P_{5/2}$	110.58	110.70	110.3	110.62	1.79(9)	1.79(9)
$2s^2 2p^3 2P_{3/2}$	$2s 2p^4 4P_{1/2}$	150.69	150.98	149.4		8.40(7)	8.58(7)
$2s^2 2p^3 2P_{3/2}$	$2s 2p^4 4P_{3/2}$	153.22	153.60	152.0		4.10(8)	4.41(8)
$2s^2 2p^3 2P_{3/2}$	$2s 2p^4 4P_{5/2}$	252.46	253.41	250.1		9.27(6)	1.03(7)

to calculate energies for 20 low-lying levels and transition probabilities for the 35 transitions. We see from Table V that our MCDF data for wavelengths agree better with experimental values given in [8] than with data from [1]. As can be seen from Table V, it is clear that the calculated values including the CV correlation are in general in very good agreement with MCDF calculations of Aggarwal et al. [1] except for some transitions with a maximum difference of approximately 1.756%, but the maximum difference for our VV correlation calculations is 0.438%. A comparison between the present wavelengths and the

JET tokamak experimental values of Denne et al. [8] reveals that the greatest difference between the experimental results and our GRASP2K transition wavelengths for our CV correlation calculations is 0.109% and the maximum difference for the results of VV correlation calculations is 0.188%. Such extrapolations are best achieved by studying the  $Z$  dependence of the difference between experimental and theoretical transition wavelengths. Further experimental confirmation would be very helpful in verifying the correctness of these occasionally sensitive mixing parameters.

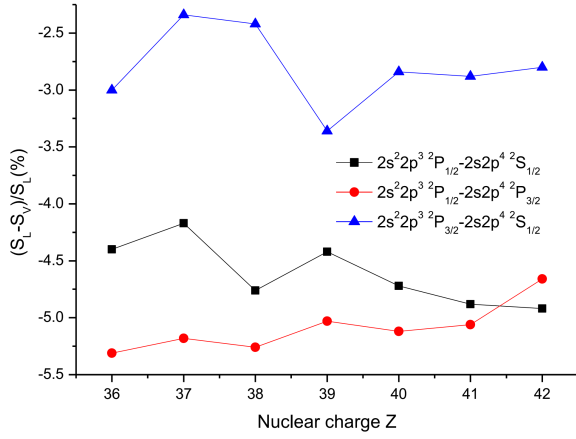


Fig. 1.  $Z$ -dependence of the ratio  $(S_L - S_V)/S_L$  in %, where line strengths  $S$  are calculated in length  $S_L$  and velocity  $S_V$  forms.

In Table VI, wavelengths and transition probabilities are presented for transitions in  $N$ -like Rb and Sr. In view of the VV and CV correlation independence just discussed, our wavelengths and transition probabilities results are presented in CV correlation form only. We limit the table to those transitions given in [4]. We see from Table VI that the agreement between our MCDF wavelengths and the NIST data from [4] is about 0.106–1.201% for Rb(XXXI) and increases with the increasing  $Z$  to 0.175–1.756% for Sr(XXXII). We found disagreement between our MCDF results and the NIST data from [4] for the  $2s^2 2p^3 4S_{3/2} - 2s 2p^4 2S_{1/2}$ ,  $2s^2 2p^3 4D_{3/2} - 2s 2p^4 2S_{1/2}$ ,  $2s^2 2p^3 2P_{1/2} - 2s 2p^4 2S_{1/2}$  and  $2s^2 2p^3 2P_{3/2} - 2s 2p^4 2S_{1/2}$  transition in Rb(XXXI). This disagreement could be caused by the difference in identification of levels. To avoid future level identification problems, we include in Table VI not only wavelengths but also transition rates. Our GRASP2K calculation of the  $A$  value for the  $2s^2 2p^3 - 2s 2p^4$  transition is in excellent agreement with the recommended data from [4]. Finally, we expect our values to be more accurate than the MCDF results from [4] for the transitions presented in Table VI since VV and CV correlation corrections as well as retardation are included in our calculations.

In Fig. 2, we compare the theoretical data from [1, 3, 10, 11] with our theoretical values. The trend of the other theoretical results follows the theoretical predictions (VV) fairly well. It should be noted that the data given in [1, 3, 10, 11] provided the first systematic study of transition rates ratios and served as a probe of intermediate coupling in the  $N$ -like system.

The contributions of different configurations to the weighted sum of configuration-average energy levels are illustrated in Figs. 3 and 4, where the variation with  $Z$  of the Breit interaction (B) self-energy (SE) and vacuum polarization (V) are shown for the  $2s^2 2p^3$  ground state and  $2s 2p^4$  final state. As seen in Figs. 3 and 4, the results indicate that both the Breit interaction and self-energy modifications are prominent, and we can see that self-

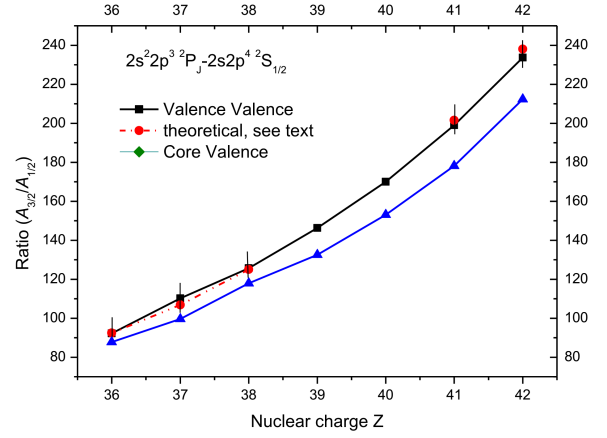


Fig. 2. Branching ratios:  $A_{3/2}/A_{1/2}$  for transitions  $2s^2 2p^3 2P_J - 2s 2p^4 2S_{1/2}$  from different correlation effects, plotted as the difference in other theoretical ratios compared to our calculations. The theoretical ratios are from Refs. [1, 3, 10–11].

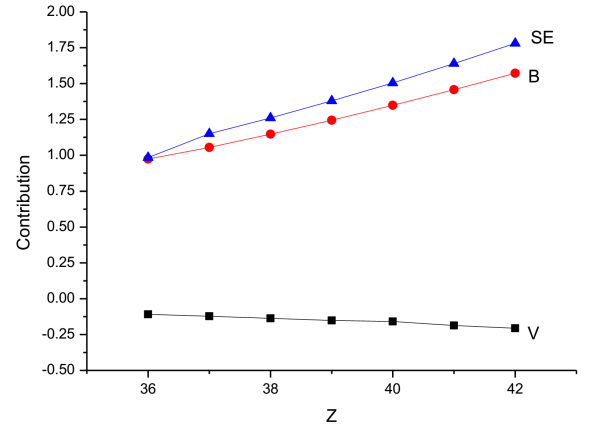


Fig. 3. Contributions to the weighted sum of configuration-average energy levels of the final configurations in  $N$ -like isoelectronic sequence from the Breit interaction (B), self-energy (SE) and vacuum polarization (V).

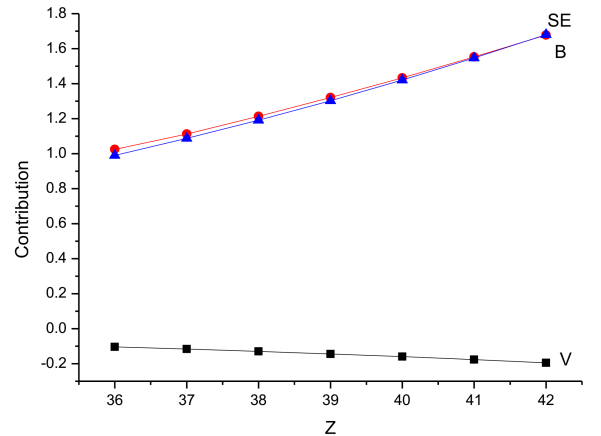


Fig. 4. Contributions to the weighted sum of configuration-average energy levels of the ground configurations in  $N$ -like isoelectronic sequence from the Breit interaction (B), self-energy (SE) and vacuum polarization (V).

energy occupies a large weight in QED corrections. With the increasing number of charges, the Breit energy increases whereas self-energy changes little and vacuum polarization is nearly a constant. This can be explained as follows: compared with highly ionized ions, in low-charge

state ions and neutral atoms the nuclear charge  $Z$  is nearly equal to the number of electrons, the repulsive force between electrons and nuclear electrostatic attraction become larger, and therefore the electron correlation becomes important with increasing atomic number  $Z$ .

TABLE VI

Wavelengths  $\lambda$  [Å] and transition probabilities  $A$  [ $s^{-1}$ ] for LS-allowed transitions in Sr(XXXII) and Rb(XXXI): (a) present, (b) MCDF data [4]. The number in brackets represents the power of 10.

Lower Level	Upper Level	Sr(XXXII)				Rb(XXXI)			
		$\lambda^a$ (CV)	$A^a$	$\lambda^b$	$A^b$	$\lambda^a$ (CV)	$A^a$	$\lambda^b$	$A^b$
$2s^2 2p^3 4S_{3/2}$	$2s 2p^4 2S_{1/2}$	31.36	3.77(7)	31.26	3.97(7)	33.82	3.76(7)		
$2s^2 2p^3 2D_{3/2}$	$2s 2p^4 2S_{1/2}$	37.13	2.98(10)	37.00	3.31(10)	39.69	2.96(10)		
$2s^2 2p^3 4S_{3/2}$	$2s 2p^4 2P_{3/2}$	37.75	1.71(10)	37.54	1.86(10)	40.36	1.67(10)	40.12	1.82(10)
$2s^2 2p^3 2P_{1/2}$	$2s 2p^4 2S_{1/2}$	41.57	2.28(9)	40.84	2.32(9)	44.01	2.20(9)		
$2s^2 2p^3 4S_{3/2}$	$2s 2p^4 2D_{5/2}$	41.81	4.98(7)	41.68	4.74(7)	44.90	4.49(7)	44.75	4.18(7)
$2s^2 2p^3 4S_{3/2}$	$2s 2p^4 2D_{3/2}$	44.47	2.16(10)	44.34	2.50(10)	47.69	2.19(10)	47.53	2.52(10)
$2s^2 2p^3 2D_{3/2}$	$2s 2p^4 2P_{3/2}$	46.43	2.75(8)	46.13	2.47(8)	49.00	5.54(8)	48.67	7.07(8)
$2s^2 2p^3 2D_{5/2}$	$2s 2p^4 2P_{3/2}$	48.97	2.51(11)	48.67	2.71(11)	51.73	2.30(11)	51.39	2.48(11)
$2s^2 2p^3 2P_{3/2}$	$2s 2p^4 2S_{1/2}$	51.41	2.69(11)	51.10	2.90(11)	54.27	2.44(11)		
$2s^2 2p^3 2P_{1/2}$	$2s 2p^4 2P_{3/2}$	52.74	4.27(10)	52.27	4.55(10)	55.77	3.74(10)	55.24	3.99(10)
$2s^2 2p^3 2D_{3/2}$	$2s 2p^4 2D_{5/2}$	52.72	2.18(9)	52.54	2.30(9)	55.86	1.76(9)	55.65	1.85(9)
$2s^2 2p^3 4S_{3/2}$	$2s 2p^4 4P_{1/2}$	53.04	9.42(10)	52.97	1.01(11)	56.53	8.18(10)	56.45	8.79(10)
$2s^2 2p^3 4S_{3/2}$	$2s 2p^4 4P_{3/2}$	53.16	1.25(11)	53.03	1.32(11)	56.77	1.04(11)	56.65	1.09(11)
$2s^2 2p^3 2D_{5/2}$	$2s 2p^4 2D_{5/2}$	56.03	9.43(10)	55.86	1.02(11)	59.43	8.46(10)	59.24	9.18(10)
$2s^2 2p^3 2D_{3/2}$	$2s 2p^4 2D_{3/2}$	57.02	1.11(11)	56.84	1.20(11)	60.25	1.02(11)	60.02	1.11(11)
$2s^2 2p^3 2D_{5/2}$	$2s 2p^4 2D_{3/2}$	60.92	5.61(9)	60.8	5.85(9)	64.42	4.96(9)	64.22	5.14(9)
$2s^2 2p^3 4S_{3/2}$	$2s 2p^4 4P_{5/2}$	63.26	2.62(10)	63.24	2.79(10)	67.44	2.38(10)	67.42	2.55(10)
$2s^2 2p^3 2P_{1/2}$	$2s 2p^4 2D_{3/2}$	66.76	2.17(9)	66.5	2.48(9)	70.82	2.22(9)	70.34	2.55(9)
$2s^2 2p^3 2P_{3/2}$	$2s 2p^4 2P_{3/2}$	71.14	1.56(10)	70.3	1.62(10)	73.34	1.46(10)	72.46	1.56(10)
$2s^2 2p^3 2D_{3/2}$	$2s 2p^4 4P_{1/2}$	71.93	2.18(9)	71.8	2.52(9)	75.07	2.27(9)	74.99	2.59(9)
$2s^2 2p^3 2D_{3/2}$	$2s 2p^4 4P_{3/2}$	72.14	3.64(8)	72.0	3.45(8)	75.50	7.42(7)	75.34	7.58(7)
$2s^2 2p^3 2D_{5/2}$	$2s 2p^4 4P_{3/2}$	78.48	5.04(9)	78.3	4.94(9)	82.17	3.82(9)	82.08	3.71(9)
$2s^2 2p^3 2P_{3/2}$	$2s 2p^4 2D_{5/2}$	86.58	1.04(10)	86.4	1.06(10)	89.84	9.39(9)	89.10	1.02(10)
$2s^2 2p^3 2P_{1/2}$	$2s 2p^4 4P_{3/2}$	88.33	1.59(8)	88.1	1.74(8)	92.86	1.38(8)	92.35	1.48(8)
$2s^2 2p^3 2D_{3/2}$	$2s 2p^4 4P_{5/2}$	92.12	7.73(9)	92.1	7.96(9)	95.63	6.79(9)	95.67	7.29(9)
$2s^2 2p^3 2P_{3/2}$	$2s 2p^4 2D_{3/2}$	99.47	4.98(7)	98.7	4.71(7)	101.76	8.10(6)	100.87	8.19(6)
$2s^2 2p^3 2D_{5/2}$	$2s 2p^4 4P_{5/2}$	102.72	2.31(9)	102.9	2.39(9)	106.59	2.05(9)	106.79	2.11(9)
$2s^2 2p^3 2P_{3/2}$	$2s 2p^4 4P_{1/2}$	155.49	7.25(7)	154.8	7.85(7)	152.66	7.93(7)	151.79	8.51(7)
$2s^2 2p^3 2P_{3/2}$	$2s 2p^4 4P_{3/2}$	156.49	3.32(8)	155.3	3.87(8)	154.45	3.76(8)	153.23	4.40(8)
$2s^2 2p^3 2P_{3/2}$	$2s 2p^4 4P_{5/2}$	296.51	4.92(6)	295	5.79(6)	270.12	8.07(6)	269.83	8.31(6)

#### 4. Conclusions

We have investigated the effect of core-valence correlation, Breit interaction and QED effects on the atomic state function and corresponding energy of the  $N$ -like  $2s^2 2p^3 - 2s 2p^4$  transitions in the ions Kr(XXX)-Sr(XXXII). The MCDHF gives excellent agreement with experimental data and adopted results. It would be beneficial if experimental data for other highly charged  $N$ -like ions were available. At the present time, there are no experimental data between  $Z = 37$  and  $Z = 38$  for the

nitrogen isoelectronic sequence. Availability of such data would lead to an improved understanding of the relative importance of different contributions to the energies of highly charged ions. These calculations provide a theoretical benchmark for comparison with experiment and theory. In this calculation (see Tables I-VI), it is clear that the MCDF method, including the core-valence correlation, is an accurate approach for the whole sequence. It is in general clear that the relativistic and configuration interaction effects play important roles in the correct

assignment of different transitions and also in the accurate evaluation of atomic transition data of highly ionized atoms. Finally, we believe that the present results are the most extensive and definitive to date and should be useful in many astrophysical applications, particularly that previously unavailable data are also presented.

### Acknowledgments

The authors are grateful to P. Jönsson for providing the GRASP2K package and ATSP2K package and giving us many useful instructions.

### References

- [1] K.M. Aggarwal, F.P. Keenan, K.D. Lawson, *At. Data Nucl. Data Tables* **94**, 323 (2008).
- [2] J. Huang, G. Jiang, Q. Zhao, *Chin. Phys. Lett.* **23**, 69 (2006).
- [3] K.T. Cheng, Y.-K. Kim, J.P. Desclaux, *At. Data Nucl. Data Tables* **24**, 111 (1979).
- [4] H.L. Zhang, D.H. Sampson, *At. Data Nucl. Data Tables* **72**, 153 (1999).
- [5] G.C. Rodrigues, P. Indelicato, J.P. Santos, P. Patté, F. Parente, *At. Data Nucl. Data Tables* **86**, 117 (2004).
- [6] M.F. Gu, *At. Data Nucl. Data Tables* **89**, 267 (2005).
- [7] I. Kink, J.M. Laming, E. Takács, J.V. Porto, J.D. Gillaspy, E. Silver, H. Schnopper, S.R. Bandler, M. Barbera, N. Brickhouse, S. Murray, N. Madden, D. Landis, J. Beeman, E.E. Haller, *Phys. Rev. E* **63**, 046409 (2001).
- [8] B. Denne, E. Hinnov, J. Ramette, B. Saoutic, *Phys. Rev. A* **40**, 1488 (1989).
- [9] E.B. Saloman, *J. Phys. Chem. Ref. Data* **36**, 1 (2007).
- [10] J.E. Sansonetti, *J. Phys. Chem. Ref. Data* **35**, 1 (2006).
- [11] J.E. Sansonetti, *J. Phys. Chem. Ref. Data* **41**, 1 (2012).
- [12] L.-H. Hao, G. Jiang, S.-Q. Song, F. Hu, *At. Data Nucl. Data Tables* **94**, 739 (2008).
- [13] I.P. Grant, *Relativistic Quantum Theory of Atoms and Molecules*, Springer, New York 2007.
- [14] I.P. Grant, B.J. McKenzie, P.H. Norrington, D.F. Mayers, N.C. Pyper, *Comput. Phys. Commun.* **21**, 207 (1980).
- [15] P. Jönsson, X. He, C. Froese Fischer, I.P. Grant, *Comput. Phys. Commun.* **177**, 597 (2007).
- [16] F.A. Parpia, C. Froese Fischer, I.P. Grant, *Comput. Phys. Commun.* **94**, 249 (1996).
- [17] J. Olsen, M.R. Godefroid, P.A. Jonsson, P.A. Malmquist, F.C. Froese, *Phys. Rev. E* **52**, 4499 (1995).
- [18] M. Huang, M. Andersson, T. Brage, R. Hutton, P. Jönsson, C.C. Yang, Y.M. Zou, *J. Phys. B At. Mol. Opt. Phys.* **38**, 503 (2005).
- [19] M.F. Gu, *Astrophys. J.* **582**, 1241 (2003).
- [20] NIST: <http://physics.nist.gov/PhysRefData>.